A near-wall patch wall model for large-eddy simulation

By A. Elnahhas, A. Lozano-Durán† AND P. Moin

1. Motivation and objectives

The direct numerical simulation (DNS) of high-Re wall-bounded turbulent flows is prohibitively expensive, with its cost scaling as $Re_\tau^{5/2}$ in channel flows, where Re_τ is the Reynolds number defined based on the friction velocity (Mizuno & Jiménez 2013). The direct application of the large-eddy simulation (LES) approach, where only the energy-containing eddies are resolved, to wall-bounded turbulent flows, termed wall-resolved LES (WRLES), yields a marginally better cost scaling than DNS, Re_τ^2 (Mizuno & Jiménez 2013). The still prohibitive cost of WRLES is due to the reduction in size of the energy-containing eddies as the wall is approached (Tennekes & Lumley 1972; Townsend 1976). Wall-modeled LES (WMLES) attempts to further reduce the cost by only resolving the energy-containing eddies in the outer region of the flow, extending the near-isotropic grid which scales in outer units to the wall. The effect of the severely under-resolved near-wall region on the outer flow is replaced by wall models (Bose & Park 2018). The cost scaling of WMLES is potentially reduced to Re_τ^0 assuming the same arguments made by Choi & Moin (2012) and Yang & Griffin (2021) in the context of spatially-evolving boundary layers.

The wall models employed in WMLES rely primarily on some form of the Reynolds-averaged Navier-Stokes (RANS) equations (Bose & Park 2018). This could range from the entirety of the RANS equations solved on a separate embedded grid such as the non-equilibrium wall model (NEQWM) of Park & Moin (2014) to the equilibrium wall model (EQWM), where all terms in the RANS equations are ignored except for the wall-normal diffusion, equivalent to the assumptions of local equilibrium and a constant stress layer. The use of the RANS equations limits the predictive capabilities of these wall models to the mean wall-shear stress, with higher-order statistics and fluctuating quantities such as the wall-shear stress fluctuations being severely underpredicted, regardless of grid refinement (Park & Moin 2016). This is expected, because the near-wall eddies responsible for the wall-shear stress fluctuations are under-resolved and not modeled explicitly. Furthermore, the use of the gradient-diffusion hypothesis to model the Reynolds shear stress in both the EQWM and NEQWM prevents them from behaving correctly under viscously induced three-dimensional non-equilibrium effects (Lozano-Durán *et al.* 2020). This is due to the misalignment between the mean shear and the Reynolds shear stress.

The objective of this study is to devise a wall model that incorporates the near-wall turbulent structures, hence addressing the misprediction of both the wall-shear stress fluctuations and the non-equilibrium behavior of the near-wall layer. To do so, we propose to use a near-wall patch with DNS resolution. The patch has a size that is constant in inner units in all three Cartesian directions and is independent of the LES grid size. To couple the patch to the outer LES flow, we utilize the wall-normal self-similar structure

† Massachusetts Institute of Technology

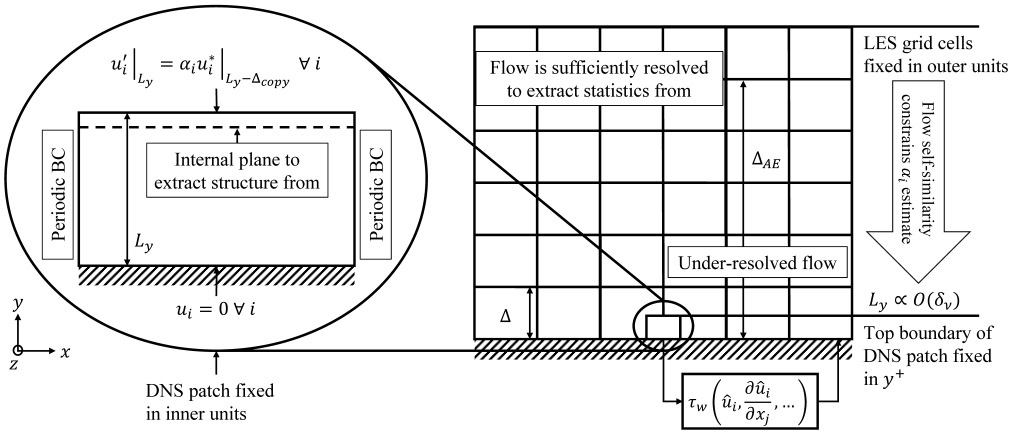

FIGURE 1. Schematic showing the interdependence of the DNS near-wall patch and the outer-flow LES flow field. The near-wall patch is fixed in inner units, and its size is independent of the LES grid size. The outer flow centered around Δ_{AE} is used to extract statistical constraints that are enforced at the top boundary of the DNS near-wall patch. The inset shows the boundary conditions (BC) of the DNS near-wall patch, where the dashed line indicates the internal plane whose structure is copied and rescaled at the top boundary (Elnahhas *et al.* 2020).

of high-Re_τ wall-bounded turbulent flows, namely the presence of a self-similar hierarchy of wall-attached eddies scaling with distance from the wall (Townsend 1976; Marusic & Monty 2019). Below the smallest eddies in this self-similar hierarchy, there is a near-wall self-sustaining cycle (Jiménez & Pinelli 1999). The patch is sized such that it captures the smallest eddies in the self-similar hierarchy of wall-attached eddies. Because the outer LES flow captures the largest eddies in the hierarchy, a coupling between the two domains motivated by the attached-eddy hypothesis is pursued. It is argued that such an approach leads the cost of the wall model to scale as Re_τ^0. Other approaches that utilize patches have linked their size to the LES grid size, resulting in less-favorable cost scalings (Sandham *et al.* 2017).

Another approach motivated by the self-similar hierarchy of wall-bounded turbulent structures is the multi-block method of Pascarelli *et al.* (2000), who also suggested using periodically replicated subdomains that are constant in size in inner units. However, these subdomains were coupled directly to the outer flow, and required a hierarchy of them to be explicitly added and inter-coupled as Re_τ increased. In this study, the use of the attached-eddy hypothesis to couple the near-wall patch with the outer LES domain can be viewed as a method to circumvent hierarchical domains of Pascarelli *et al.* (2000). Figure 1 illustrates all the components of the proposed coupling.

The remainder of this study is structured as follows. Section 2 presents the formulation of the DNS near-wall patch wall model (NWP-WM) along with an attached-eddy-based coupling between it and the outer LES domain. In Sections 3 and 4, the results of using the NWP-WM in both equilibrium and non-equilibrium channel flows, respectively, are presented. Finally, conclusions are drawn and future tasks are presented in Section 5. This study extends the work presented by Elnahhas *et al.* (2020).

2. The near-wall patch wall model formulation

The near-wall patch is intended to capture the smallest of the wall-normal self-similar eddies. Combined with the outer LES capturing the largest of the self-similar eddies, the ones in between can be accounted for with statistical constraints. This alleviates the need for a hierarchy of patches as described in Pascarelli *et al.* (2000).

2.1. *A near-wall patch constant in inner units*

Let x, y, and z denote the streamwise, wall-normal, and spanwise coordinates, respectively, with u, v, and w denoting the corresponding velocity components in each direction. In index notation, these correspond to $i = 1, 2, \text{and } 3$, respectively. As discussed by Elnahhas *et al.* (2020), consider a region near the wall that is homogeneous in the wall-parallel directions, The wall-parallel averaged wall-shear stress $\overline{\tau_w}^{x,z}$ can be used to find a time-varying friction velocity $u_\tau(t) = (\overline{\tau_w}^{x,z}/\rho)^{1/2}$, where $\overline{(.)}^{x,z}$ denotes averaging along the homogeneous directions, and ρ is the fluid density. Rescaling continuity and the Navier-Stokes equations with this time-dependent friction velocity, while maintaining time in outer units, leads to

$$\frac{\partial u_i^+}{\partial x_i^+} = 0, \tag{2.1}$$

$$\frac{\partial u_i^+}{\partial t} = \frac{u_\tau^2(t)}{\nu}\left(- \frac{\partial u_i^+ u_j^+}{\partial x_j^+} - \frac{\partial p^+}{\partial x_i^+} + \frac{\partial^2 u_i^+}{\partial x_j^+ \partial x_j^+}\right) - u_i^+ \frac{1}{u_\tau}\frac{du_\tau}{dt} \equiv R_i + A(t)u_i^+, \tag{2.2}$$

where $(.)^+$ indicates time-dependent plus units, and R_i are all the terms on the right-hand side (RHS) of the momentum equation, excluding the linear forcing term. The linear forcing term $A(t)u_i^+$ is required to force the size of the patch to remain constant in inner units.

As opposed to Elnahhas *et al.* (2020), the time under which the patch evolves is retained in outer units for two reasons. First, because the patch is coupled to the outer LES, it is more convenient to maintain the same time for both simulation domains. Second, and more importantly, note that $u_\tau \equiv u_\tau(t)$ is measured in physical time, and it is used to define the inner unit time-scale, $t^+ = tu_\tau^2(t)/\nu$. If instead we define $u_\tau \equiv u_\tau(t^+)$, then there is the potential for u_τ to be multi-valued in physical time when coupling back the wall-shear stress predicted by the patch to the LES domain. To understand this, consider the case of temporally intermittent, large wall-shear stress fluctuations averaged along the wall-parallel directions inside the patch. If the temporal fluctuation of this local mean wall-shear stress is strong enough, the conversion from $t^+ \longrightarrow t = t^+\nu/u_\tau^2(t^+)$ could lead to a smaller value of t than before, which is unphysical.

To maintain the size of the patch in inner units, the linear forcing term on the RHS of Eq. (2.2) is used to enforce the implicit constraint of $\partial\overline{u^+}^{x,z}/\partial y^+|_w = 1$, which follows from the definition of plus units. The friction velocity $u_\tau(t)$ can be found by integrating

$$\frac{du_\tau}{dt} = -A(t)u_\tau \tag{2.3}$$

alongside the governing equations, using an appropriate definition of $A(t)$. A proportional controller is used similar to that of Bassenne *et al.* (2016). Averaging the streamwise component of Eq. (2.2) along the wall-parallel directions and evaluating the wall-normal

derivative at the wall leads to the equation

$$\frac{\partial}{\partial t}\left(\frac{\partial \overline{u^+}^{x,z}}{\partial y^+}\bigg|_w\right) = \frac{\partial \overline{R_1}^{x,z}}{\partial y^+}\bigg|_w + A(t)\frac{\partial \overline{u^+}^{x,z}}{\partial y^+}\bigg|_w \tag{2.4}$$

for the time evolution of the slope at the wall of the mean streamwise velocity.

By equating the RHS of this evolution equation to a proportional controller, an expression for $A(t)$ is found,

$$A = \frac{\frac{\partial \overline{R_1}^{x,z}}{\partial y^+}\big|_w - \frac{G}{\tau_\infty^+}\left(\frac{\partial \overline{u^+}^{x,z}}{\partial y^+}\big|_w - 1\right)}{\frac{\partial \overline{u^+}^{x,z}}{\partial y^+}\big|_w}, \tag{2.5}$$

where τ_∞^+ is the large-eddy turnover time inside in the patch, which is proportional to its size in inner units, and τ_∞^+/G is some time constant chosen to be smaller than the Kolmogorov timescale of the patch in inner units (i.e., $\tau_\infty^+/G < \tau_\eta^+ = 1$). For all cases in this study, this time constant is chosen to be 0.4, with no variation in the results found with time constants as low as 0.04.

In the case where the flow is not aligned with the streamwise coordinate direction, such as the case of the temporally varying three-dimensional non-equilibrium channel flow of Lozano-Durán *et al.* (2020), a similar approach is used to derive the proportional controller, where the implicit constraint is the resultant wall-normal slope

$$\sqrt{\left(\frac{\partial \overline{u^+}^{x,z}}{\partial y^+}\right)^2 + \left(\frac{\partial \overline{w^+}^{x,z}}{\partial y^+}\right)^2} = 1. \tag{2.6}$$

2.2. *The size of the patch in inner units*

The size of the patch is important for the justification of the attached-eddy-based top BC, and the coupling procedure to the outer flow (Elnahhas *et al.* 2020). Because the patch needs to adequately represent the near-wall self-sustaining cycle, any Re_τ-invariant dynamics, as well as the smallest of the self-similar attached eddies, its size in all three coordinate directions should be chosen accordingly. High-pass filtering the turbulent kinetic energy shows that the near-wall region has an Re_τ-invariant solution for wavelengths shorter than $\lambda_{x,z}^+ \approx 1000$ (Lee & Moser 2019). Following the choice of Carney *et al.* (2020), the patch is chosen to have a size of $(L_x^+, L_y^+, L_z^+) = (1500, 300, 1500)$. The following subsection shows that wall-normal self-similarity starts to emerge around $y^+ \approx 100$, indicating that the wall-normal height of the patch satisfies the constraint of containing the smallest of the self-similar wall-attached eddies. Finally, the aspect ratio of this patch is consistent with the aspect ratios of wall-attached self-similar eddies (Lozano-Durán & Bae 2019; Chandran *et al.* 2020).

2.3. *The top boundary condition of the patch*

The near-wall patch is homogeneous in the x and z directions, and periodic boundary conditions are applied to all velocity components. In the wall-normal direction, the no-slip and no-penetration boundary conditions are applied at the bottom wall. At the top of the patch, the mean and fluctuating components of each of the three velocity components are specified separately as follows

$$u_i^+|_{L_y^+} = \overline{u}_i^+|_{L_y^+} + u_i^{+'}|_{L_y^+}. \tag{2.7}$$

Following Elnahhas *et al.* (2020), the mean velocities in the wall-parallel directions are specified by assuming the existence of a logarithmic profile between the outer LES flow around Δ_{AE} and the top of the patch. The von Kármán constant and the intercept of the log-law are dynamically found using a least-squares approach centered around Δ_{AE}. The fluctuating component of each of the velocities is defined using a magnitude, α_i, and a spatial structure function, u_i^* as follows

$$u_i^{+'}|_{L_y^+} = \alpha_i u_i^*(x^+, z^+)|_{L_y^+}. \tag{2.8}$$

At a sufficiently high Re_τ, the wall-attached eddies carry the bulk of the turbulent kinetic energy and momentum of the flow (Townsend 1976; Perry & Chong 1982; Marusic & Monty 2019). Under these assumptions, the turbulent intensity profiles reduce to logarithmic forms

$$\frac{\overline{u'^2}}{u_\tau^2} = B_1 - A_1 \log\left(\frac{y}{\delta}\right), \quad \frac{\overline{w'^2}}{u_\tau^2} = B_2 - A_2 \log\left(\frac{y}{\delta}\right), \quad \frac{\overline{v'^2}}{u_\tau^2} = B_3, \tag{2.9}$$

where A_1, A_2, B_1, B_2, and B_3 are coefficients that depend on the flow, and δ is the channel half-height or boundary layer thickness. By fitting these coefficients dynamically using a least-squares approach centered around Δ_{AE}, the scaling magnitudes α_i can be specified using the extrapolated values of $\overline{u_i'^2}+$ at L_y^+.

As discussed by Elnahhas *et al.* (2020), the self-similar hierarchy extends beneath the top boundary of the patch, and as such, the spatial structure of the top boundary condition is based on a rescaling of the flow inside the patch. Several boundary conditions were tested by running the patch in an *a-priori* setting similar to that of Elnahhas *et al.* (2020). These included copying the structure of a plane a certain distance away from the top boundary, rescaling the Fourier components of the plane in wavenumber space using the difference between the characteristic shear length scale $\ell^* = u_\tau/(\partial\overline{u^+}^{x^+,z^+}/\partial y^+)$ at the copying plane and the top boundary while accounting for the difference in mean advection velocities, filtering global wall-normal velocity components, and accounting for virtual origins of the self-similar scaling (Lozano-Durán & Bae 2019; Mizuno & Jiménez 2013; Encinar *et al.* 2014). It was found that these choices made little difference as long as the source plane was within the logarithmic region. This is understood by considering that if the source plane was taken from $y^+ \approx 200$, any of these choices would change the scale of the resulting structures by 15% at most, which was found not to have substantial effects.

Owing to these results, and the computational complexity and cost of wavenumber rescaling, the top boundary condition used for the coupled patch-LES calculations in the subsequent sections only copies the structure of the fluctuations while accounting for the difference in mean advection velocities between the source and the top boundary condition planes. The plane was copied from $y^+ \approx 230$, and varying this location between $y^+ \approx 160{-}250$ yielded negligible changes to the mean wall shear-stress prediction, which is the primary quantity of interest.

2.4. *The cost scaling of the patch*

The nominal start of the logarithmic region of the flow scales in inner units as $2.6Re_\tau^{1/2}$ (Klewicki *et al.* 2009). If the patch is required to capture the start of the logarithmic region, then its cost would scale as $N_x \times N_y \times N_z \sim Re_\tau^{3/2}$, where N_x, N_y, and N_z are the number of grid points in the three coordinates. However, the primary constraint on the patch is to capture the smallest self-similar eddies, not the start of the logarithmic layer.

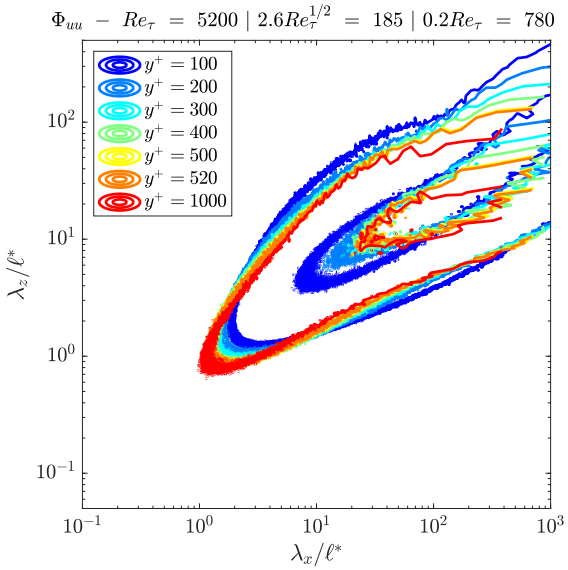

FIGURE 2. Premultiplied two-dimensional streamwise energy spectra as a function of the streamwise and spanwise characteristic shear length-normalized wavelengths for an $Re_\tau = 5200$ channel flow (Lee & Moser 2015). The contour levels are $\{0.1, 0.6\} \times \max(k_x k_z \Phi^+_{u'u'})$. The nominal start and end of the logarithmic layer are shown above the plot (Klewicki *et al.* 2009).

If the smallest of the self-similar eddies are fixed in size in inner units, that would make the cost of the scale as Re_τ^0. To verify if that is the case, we examine the premultiplied two-dimensional spectra of the one of the highest available Re_τ channel flows, namely the $Re_\tau = 5200$ of Lee & Moser (2015).

Figure 2 shows the premultiplied two-dimensional spectra of the streamwise turbulence intensity as a function of wall-normal height. The figure shows that when normalized by the characteristic shear length scale ℓ^*, the spectra collapse across the entirety of the logarithmic region, which is bounded from below by $2.6Re_\tau = 185$, and from by above by $0.2Re_\tau = 780$. However, it is evident that there is approximate collapse below the lower bound as well, down to $y^+ = 100$. This behavior is observed at lower-Re_τ channel flows down to $Re_\tau = 1000$. However, the $Re_\tau = 5200$ result is most important because it is the value where the separation between the nominal start of the logarithmic region and the closest collapsing contours to the wall is largest. This result confirms that the cost of the patch is nominally Re_τ^0.

However, note that while the self-similar rescaling or copying of the structure of the interior of the patch remains valid as Re_τ increases, the statistical constraints in Eq. (2.9) lose their validity due to the increase in size of the mesolayer. More refined expressions, such as those derived by Chen *et al.* (2018), are necessary for accurate prediction of the scaling magnitudes.

2.5. *The outer flow grid requirement*

Since the coupling between the outer LES and the patch requires an accurate prediction of the turbulent intensities in the outer regions of the logarithmic region, the outer LES has to be sufficiently resolved. Lozano-Durán & Bae (2019) showed that a grid resolution

Domain	N_x	N_y	N_z	Δ_x^+	Δ_z^+	Δ_y^+	$L_x^{(+)}$	$L_y^{(+)}$	$L_z^{(+)}$	Δ_{copy}^+	Δ^{AE}	SGS model
Patch	256	66	256	5.9	5.9	0.38-7.4	1500	300	1500	230	0.1-0.2δ	-
LES	256	121	128	100	100	35-100	$2\pi\delta$	2δ	$\pi\delta$	-	-	AMD

TABLE 1. Mesh parameters for the patch and the outer LES domains at $Re_\tau = 4200$. Note that the patch domain size and resolution are fixed in inner units independent of Re_τ while those of the outer LES are fixed in outer units. Δ^{AE} corresponds to the region in the outer LES where the logarithmic mean velocity and turbulent intensity functional forms are fitted using least squares. Δ_{copy}^+ corresponds to the wall-normal height of the plane whose structure is copied for the top boundary condition. The grid resolution for the EQWM case is the same as that used for the outer LES coupled to the patch, and the EQWM matching location is the third grid point away from the wall, corresponding to $y^+ \approx 90$. The subgrid-scale (SGS) model used in the outer LES is the anisotropic minimum dissipation (AMD) model and is kept constant for both the EQWM and the patch calculations (Rozema *et al.* 2015).

satisfying the following constraints

$$\frac{2\Delta_x^{min}}{y} \approx 0.15, \quad \frac{2\Delta_z^{min}}{y} \approx 0.15, \tag{2.10}$$

where Δ_x and Δ_z are the grid sizes in the streamwise and spanwise directions, respectively, is required to resolve 90% of the turbulent kinetic energy at some wall-normal height. Applying this condition to the outer portion of the logarithmic region, $y \leq 0.2\delta$, and assuming an isotropic grid, as is the norm in WMLES, leads to a wall-normal grid resolution requirement of approximately 60 points per boundary-layer thickness. While this maybe prohibitive for external aerodynamic applications, it is lower than the accepted grid requirements of atmospheric boundary layer simulations (Ghate & Lele 2017; Howland *et al.* 2020). However, this number can be reduced if wall-normal stretching is employed outside the logarithmic region, and if the required resolved turbulent intensity for an accurate prediction of the patch's top boundary condition is lower than 90%. The second point was not investigated in this study. Regardless, because this estimate scales in outer units, it does not change the cost of scaling of WMLES discussed in Section 1.

3. Equilibrium channel flow and comparison to the EQWM

As a first test, we use the NWP-WM in a canonical equilibrium channel flow at $Re_\tau = 4200$, corresponding to the DNS of Lozano-Durán & Jiménez (2014). Table 1 shows the number of grid points, the domain size, and the resolutions for both the outer LES and the patch. Further details such as the location of the source plane for the patch boundary condition, the location in the outer LES where Eq. (2.9) is fitted using least squares, and the the SGS model used are included in the table. Note that the wall-normal grid of the outer LES is weakly stretched to deposit 15 points below $y/\delta = 0.2$, with a total of 60 points across the channel half-height. Furthermore, the wall-shear stress predicted by the near-wall patch is applied everywhere along the top and bottom walls of the LES channel, and changes only temporally. In between LES time steps, the patch is run with a CFL of 0.5 to bridge the temporal gap. For comparison, we run both the NWP-WM and the EQWM with third-point matching with equal outer LES grid resolution. Both

wall-models are run in both constant mass flux and constant pressure gradient modes to test the validity of our assumptions in predicting the correct mean-wall shear stress as compared to the EQWM as well as the wall-shear stress fluctuations when the mean-wall shear stress is fixed, respectively. For the NWP-WM cases, the initial condition for the patch is extracted from a separate simulation using the approach of Carney *et al.* (2020), where the domain is then truncated from 600 to 300 in the wall-normal direction, and the initial condition for the outer LES is extracted from the EQWM case. Finally, all cases are run for 15 large-scale eddy turnover times, $\tau_\infty = \delta/u_\tau$.

Figure 3(a) shows the mean velocities predicted by both the NWP-WM and the EQWM normalized by the DNS value of u_τ for the case of constant mass flux. The figure shows that profiles of the mean velocity in the outer LES for both cases are equally good, but that the prediction of the wall-shear stress by the NWP-WM is worse when compared to the EQWM. The u_τ^{NWP-WM} and u_τ^{EQWM} differ from the DNS values by 6% and 2%, respectively. Nonetheless, this prediction is quite impressive given the crudity of the assumptions made, and the lack of tuning of any of the parameters such as the patch size, copying plane location, and outer flow attached-eddy equations fitting range. However, the patch does predict the remainder of the mean velocity profile that is invisible to the outer LES, which is something not predicted by the EQWM, but rather fitted through the form of the eddy viscosity used. Note that the overlap between the two domains is only due to the small Re_τ value, and the method would eventually lead to the two domains separating as originally designed at higher values of Re_τ. The prediction of the inner mean velocity profile is quite accurate, with minor errors at the first three grid points closest to the top boundary. This is expected, as the turbulence has to adjust to the still artificial top boundary condition.

Beyond the mean velocity profile and the mean wall-shear stress, the patch provides a prediction of the near-wall turbulence intensities, and in general, the full flow structure near the wall, as seen in Figure 3(b). Similar to the mean velocity profile, the turbulence has to adjust to the artificial top boundary condition. Similarly, this adjustment zone is limited to the first three grid points in the cases of u'^+_{rms} and w'^+_{rms}. However, it extends deeper in the case of v'^+_{rms}. The reason for this discrepancy comes from the fact that the wall-normal velocity has to adjust strongly to continuity through its relation to pressure in the boundary condition for the pressure Poisson equation, and the direct copying of its structure from within the domain adversely impacts it more than the wall-parallel velocities. Finally, note that the consistent drop of u'^+_{rms} across its wall-normal extent could be due to two things. First, the elevated v'^+_{rms} profile is extracting energy from the streamwise direction due to their pressure-strain relationship. Second, the drop is due to the streamwise intensity being dominated by the large scale structures through amplitude superposition and modulation that do not fit in the patch domain (Marusic *et al.* 2010). The issue is probably a combination of both, with the first motivating the formulation of a less intrusive boundary condition for the wall-normal velocity, and the second motivating the development of super-domain-scale models (Colonius & Ran 2002).

Finally, we compare the root-mean-square (RMS) values and the spectra of the wall-shear stress fluctuations predicted by the EQWM and the NWP-WM to DNS. Table 2 shows the RMS values of the wall-shear stress fluctuations predicted by the two wall models when the channel is run with a constant pressure gradient. The NWP-WM recovers the wall-shear stress fluctuation RMS value within 3%, whereas the EQWM is off by 44%, showing significant improvement. To further examine this issue, we compare both the streamwise and spanwise wall-shear spectra from the two wall models to the DNS in

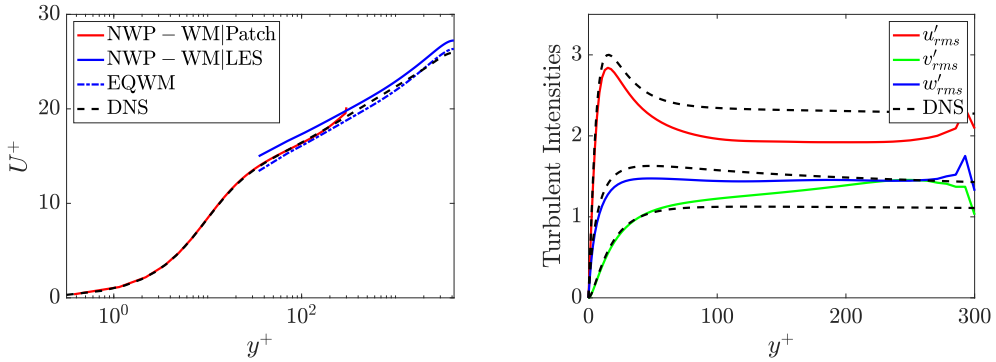

(a) (b)

FIGURE 3. (a) The streamwise mean velocity profile in inner units predicted by both the NWP-WM and the EQWM at a nominal $Re_\tau = 4200$ from the constant mass flux case calculation. The patch wall model generates two mean velocity profiles, one in the outer LES and another within the patch. (b) The turbulence intensities predicted by the near-wall patch within its domain from the constant mass flux case calculation. The solid lines represent the patch and the dashed lines represent the matching intensities from the full DNS simulations of Lozano-Durán & Jiménez (2014).

	DNS	EQWM	NWP-WM
$\tau_{w,x}^{+,rms}$	0.4413	0.2487	0.4300

TABLE 2. Fluctuating wall-shear stress root-mean-square values at $Re_\tau = 4200$ normalized in inner units. These values are from the cases run with constant pressure gradient.

Figure 4. It is evident that that EQWM captures the large scales of the wall-shear stress fluctuations reasonably well, but is not cognizant of the small-scale eddies near the wall, which contribute a substantial amount to the fluctuating wall-shear stress. In contrast, the NWP-WM does not see the larger eddies, and due to attaining local equilibrium, it is over-predicting the contribution of the smaller eddies to recover the correct RMS value, equivalent to correctly predicting the turbulent kinetic energy dissipation at the wall. However, upon rescaling the spectra predicted by the NWP-WM by $L_{(x,z)}^{Patch}/L_{(x,z)}^{LES}$, they collapse onto the DNS spectra. As such, the NWP-WM is capable of predicting both the correct RMS value, and the shape of the small-scale spectra of the wall-shear stress fluctuations. By combining both the EQWM and NWP-WM, a complete prediction of the wall-shear stress spectra across all scales is possible.

4. Non-equilibrium channel flow

To further test the capabilities of the NWP-WM, we run a case where the EQWM is known to fail, namely a viscously-induced non-equilibrium three-dimensional channel flow. In this flow, a sudden strong spanwise pressure gradient is applied to a steady two-dimensional channel flow. Depending on the strength of the transverse pressure gradient,

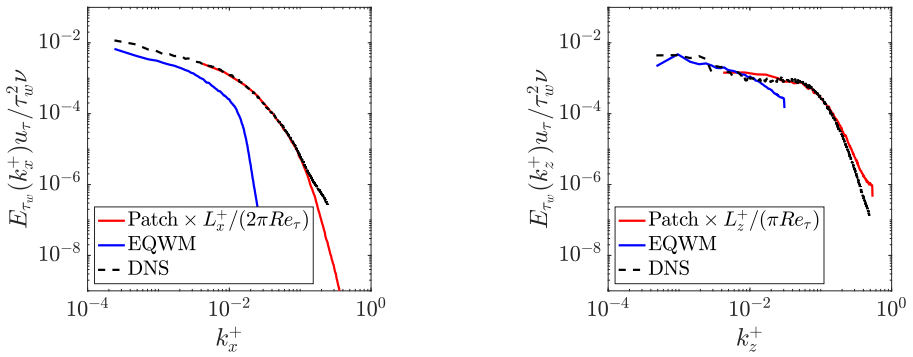

(a) (b)

FIGURE 4. (a) Streamwise (b) Spanwise wavenumber spectra of the wall-shear stress fluctuations from the constant pressure gradient case calculations. The DNS wall-shear stress fluctuations are from the DNS of Lozano-Durán & Jiménez (2014).

defined as $\Pi = (dP/dz)/(dP/dx)$, a large portion of the largest eddies in the self-similar hierarchy can be forced out of equilibrium and become misaligned with respect to the mean shear. As such, not only is the assumption of the gradient-diffusion hypothesis to model the Reynolds shear stress incorrect, but also the wall-shear stress is no longer aligned with the velocity from the matching location in the case of the EQWM. Furthermore, this misalignment is temporally varying and is intrinsically tied to the multi-scale nature of the wall-bounded flow. This case is thoroughly studied by Lozano-Durán *et al.* (2020) at the moderate $Re_\tau = 1000$. For a sufficiently high value of Π, all the wall-attached eddies are forced out of equilibrium, which corresponds to $\Pi = 420$ for our current flow with $Re_\tau = 4200$. This case is illustrated in Figure 5.

We use the two-dimensional steady-state flow of the constant streamwise pressure gradient channel solved with the NWP-WM as the initial condition. At $t = 0$, we impose a transverse pressure gradient of strength $\Pi = 420$. Flow statistics are obtained from an ensemble average of five realizations from initial conditions spaced one τ_∞ apart. Figure 6 illustrates the ensemble averaged response of the streamwise Reynolds stress and the Reynolds shear stress inside the patch. As found by Lozano-Durán *et al.* (2020), both quantities initially decay in time before eventually increasing. Comparing the numerical values and times to Figure 4 of Lozano-Durán *et al.* (2020), run at $Re_\tau = 500$, shows that the normalized response is quantitatively correct. Note that the quantities are normalized with the initial value of $u_\tau(0)$. Hence, the wall-normal extent of the patch in these original units is decreasing becuase it is held constant in inner units given the time-local value of $u_\tau(t) \equiv u_\tau^*$.

To further examine this non-equilibrium response, we compute the maximum percentage drop, $D_\tau(t^+)(Re_\tau/\Pi)$, at the wall-normal location $y^+ = 30$ defined on the basis of the initial $u_\tau(0)$. The results are shown in Figure 7(a) and are both qualitatively and numerically consistent with the predictions of Lozano-Durán *et al.* (2020). It is evident that that the eddies at $y^+ = 30$ are not affected until $t^+ \approx 30$, consistent with the idea that the smaller eddies near the wall react first to the transverse pressure gradient at a timescale proportional to their distance from the wall. Also, the normalized maximum decay and its temporal location are quantitatively consistent with the inner-layer scaling law of Lozano-Durán *et al.* (2020). However, the outer LES does not the temporal drop

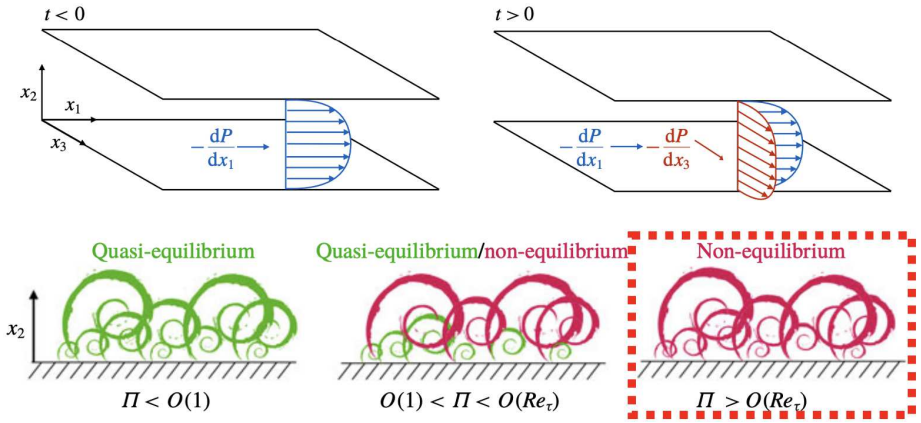

FIGURE 5. Schematic of the setup of the non-equilibrium channel flow experiment. A fully developed two-dimensional turbulent channel flow driven by $-dP/dx$ is suddenly subjected to a strong transverse pressure gradient $-dP/dz$, with the strength of the pressure gradient quantified using $\Pi = (dP/dz/dP/dx)$. The strength of the transverse pressure gradient is set to $\Pi = 420$ in this test case to drive all scales out of equilibrium, corresponding to the test case in the bottom right for a nominally $Re_\tau = 4200$ channel flow. The figure is extracted and modified from Lozano-Durán *et al.* (2020).

of the streamwise wall-shear stress. Figure 7(b) shows the output net wall-shear stress $\tau_w^* = \rho u_\tau^{*2}$, as well as its projections in the streamwise and spanwise directions, τ_w^x and τ_w^z, respectively. The streamwise wall-shear rises, then decays, followed by an eventual rise, which is inconsistent with the normalized Reynolds shear stress behavior observed by the near-wall patch. The wall-shear stress predicted by the patch is the output of the modified controller based on Eq. (2.5) for a two-dimensional, time-varying wall-shear stress. It is currently unknown whether the issue is due to the controller design, or due to some physical argument about the patch only seeing a portion of the near-wall eddies. This is a topic of current study. However, the correct quantitative normalized behavior of the eddies inside the patch indicate that the wall model may be capable of recovering the correct behavior in extremely challenging flow conditions. To date, the most sophisticated RANS-based wall model, namely the NEQWM, is incapable of capturing the non-equilibrium discussed above (Lozano-Durán *et al.* 2020).

5. Conclusions and future work

The present study builds upon the work presented by Elnahhas *et al.* (2020) where a NWP-WM is designed in such a way as to capture the near-wall self-sustaining cycle, as well as the smallest eddies in the hierarchy of wall-attached self-similar eddies, independent of the value of Re_τ and the LES grid, which scales in outer units. It is argued that such a wall model is practically necessary for the prediction of higher-order quantities of interest such as the wall-shear stress fluctuations, which are completely dependent on the near-wall structure of the flow. Furthermore, the direct capture of the near-wall eddies allows for the prediction of multi-scale phenomena such as the viscously induced three-dimensional flow, due to a sudden spanwise pressure gradient. Traditional RANS-based wall-models are known to fail in these two areas. Holding the near-wall patch constant in inner units required a controller, which was the mechanism by which the wall-shear stress was predicted. By appealing to DNS data, the sizing of the patch is chosen such

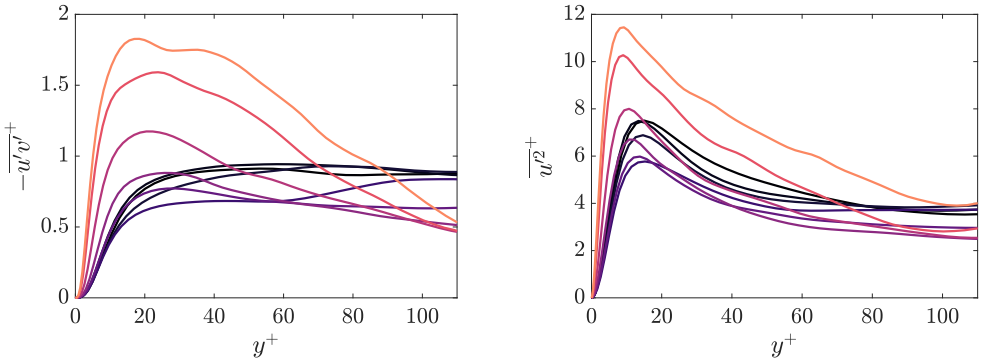

(a) (b)

FIGURE 6. The mean Reynolds stress behavior observed by the patch for the $\Pi = 420$ case at $Re_\tau = 4200$. (a) Reynold shear stress. (b) Streamwise Reynolds stress. For both plots, darker colors correspond to earlier times, while lighter colors correspond to later times with the following times $t^+ \in \{1, 30, 61, 123, 186, 248, 310, 387, 465\}$. The inner units are those normalized by the initial value of $u_\tau = u_\tau(0)$.

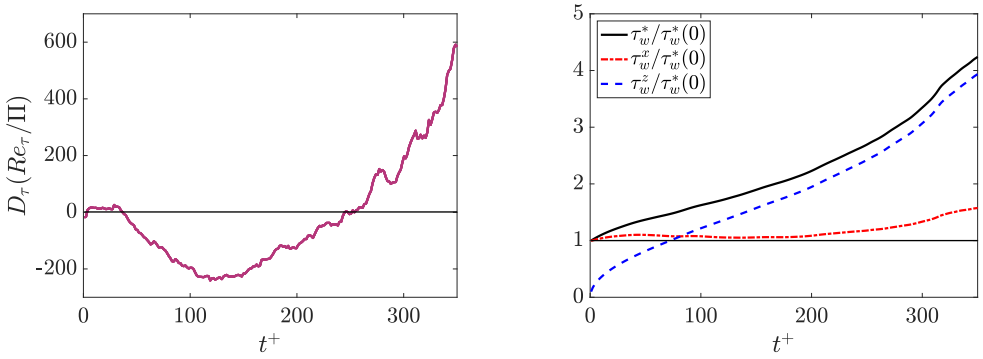

(a) (b)

FIGURE 7. (a) The maximum percentage drop of the tangential Reynolds stress at $y^+ = 30$ defined with respect to the initial value of $u_\tau = u_\tau(0)$. The maximum percentage drop is defined as $D_\tau(y^+, t) = (\overline{u'v'}(y^+, t) - \overline{u'v'}(y^+, 0))/(\overline{u'v'}(y^+, 0)) \times 100$ (Lozano-Durán *et al.* 2020). (b) The wall-shear stress predicted by the patch through the two-dimensional extended controller through Eq. (2.5)-(2.6) and outputted to the outer LES. τ_w^* is the resultant wall-shear stress, and τ_w^x and τ_w^z are the projected wall-shear stresses along the streamwise and spanwise directions, respectively. All wall-shear stresses are normalized by the fully developed two-dimensional value (thin black line).

that it captures the Re_τ-invariant dynamics of the near-wall flow as well as a portion of the self-similar flow lying above. Combined with the fact that the outer LES captures the largest of the self-similar eddies, a statistical coupling is formed using the predictions of the attached-eddy hypothesis. Even though the nominal start of the logarithmic layer is a function of Re_τ, DNS data of channel flow at $Re_\tau = 5200$ showed that the structural self-similarity starts at a location fixed in inner units, validating the formulation of the boundary condition, as well as implying that the cost scaling of such an approach is Re_τ-invariant.

The model was tested in both equilibrium and highly non-equilibrium flows. In the traditional equilibrium setting, it is capable of recovering the mean-wall shear stress value, as well as the RMS value and spatial structure of the wall-shear stress fluctuations. Furthermore, the model is capable of predicting the near-wall mean velocity profile as well as the turbulent intensities with reasonable accuracy. These are quantities of interest for multi-physics flow phenomena such as particle-laden turbulence (Johnson *et al.* 2020). In non-equilibrium settings, the near-wall patch model is capable of recovering the correct qualitative and quantitative normalized behavior of the Reynolds stress tensor, illustrating the efficacy of the multi-scale approach. However, the output wall-shear stress is mispredicted, which is currently being investigated as a potential issue of the controller design.

In future works, we will address the controller issues and verify the efficacy of the model design in highly non-equilibrium flows. Furthermore, the effect of more accurate outer flow statistical constraints will be examined. Finally, interesting research avenues such as the development of super-domain-scale models, and coupling of the EQWM and the NWP-WM for a better spatial representation of the wall-shear stress will be pursued.

Acknowledgments

This work was supported by NASA's Transformational Tools and Technologies project under grant number NNX15AU93A. The authors thank Dr. Myoungkyu Lee for sharing the two-dimensional spectra of the $Re_\tau = 5200$ channel.

REFERENCES

Bassenne, M., Urzay, J., Park, G. I. & Moin, P. 2016 Constant-energetics physical-space forcing methods for improved convergence to homogeneous-isotropic turbulence with application to particle-laden flows. *Phys. Fluids* **28**, 035114.

Bose, S. T. & Park, G. I. 2018 Wall-modeled large-eddy simulation for complex turbulent flows. *Annu. Rev. Fluid Mech.* **50**, 535–561.

Carney, S. P., Engquist, B. & Moser, R. D. 2020 Near-wall patch representation of wall-bounded turbulence. *J. Fluid Mech.* **903**, 23–24.

Chandran, D., Monty, J. P. & Marusic, I. 2020 Spectral-scaling-based extension to the attached eddy model of wall turbulence. *Phys. Rev. Fluids* **5**, 104606.

Chen, X., Hussain, F. & She, Z. 2018 Quantifying wall turbulence via a symmetry approach. Part 2. Reynolds stresses. *J. Fluid Mech.* **850**, 401–438.

Choi, H. & Moin, P. 2012 Grid-point requirements for large eddy simulation: Chapman's estimates revisited. *Phys. Fluids* **24**, 011702.

Colonius, T. & Ran, H. 2002 A super-grid-scale model for simulating compressible flow on unbounded domains. *J. Comput. Phys.* **182**, 191–212.

Elnahhas, A., Lozano-Durán, A. & Moin, P. 2020 Toward a flow-structure-based wall-modeled large-eddy simulation paradigm. *Annual Research Briefs*, Center for Turbulence Research, Stanford University, pp. 59–71.

Encinar, M. P., García-Mayoral, R. & Jiménez, J. 2014 Scaling of velocity fluctuations in off-wall boundary conditions for turbulent flows. *J. Phys. Conf. Ser.* **506**, 012002.

Ghate, A. S. & Lele, S. K. 2017 Subfilter-scale enrichment of planetary boundary layer large eddy simulation using discrete Fourier-Gabor modes. *J. Fluid Mech.* **819**, 494–539.

Howland, M. F., Ghate, A. S. & Lele, S. K. 2020 Influence of the geostrophic wind direction on the atmospheric boundary layer flow. *J. Fluid Mech.* **883**, A39.

Jiménez, J. & Pinelli, A. 1999 The autonomous cycle of near-wall turbulence. *J. Fluid Mech.* **389**, 335–359.

Johnson, P.L., Bassenne, M. & Moin, P. 2020 Turbophoresis of small inertial particles: theoretical considerations and application to wall-modelled large-eddy simulations. *J. Fluid Mech.* **883**, A27.

Klewicki, J., Fife, P. & Wei, T. 2009 On the logarithmic mean profile. *J. Fluid Mech.* **638**, 73–93.

Lee, M. & Moser, R. D. 2015 Direct numerical simulation of turbulent channel flow up to $Re_\tau \approx 5200$. *J. Fluid Mech.* **774**, 395–415.

Lee, M. & Moser, R. D. 2019 Spectral analysis of the budget equation in turbulent channel flows at high Reynolds number. *J. Fluid Mech.* **860**, 886–938.

Lozano-Durán, A. & Jiménez, J. 2014 Effect of the computational domain on direct simulations of turbulent channels up to $Re_\tau = 4200$. *Phys. Fluids* **26**, 011702.

Lozano-Durán, A. & Bae, H. J. 2019 Error scaling of large-eddy simulation in the outer region of wall-bounded turbulence. *J. Comput. Phys.* **392**, 532–555.

Lozano-Durán, A. & Bae, H. J. 2019 Characteristic scales of Townsend's wall-attached eddies. *J. Fluid Mech.* **868**, 698–725.

Lozano-Durán, A., Giometto, M. G., Park, G. I. & Moin, P. 2020 Non-equilibrium three-dimensional boundary layers at moderate Reynolds numbers. *J. Fluid Mech.* **883**, A20.

Marusic, I., Mathis, R. & Hutchins, N. 2010 Predictive model for wall-bounded turbulent flow. *Science* **329**, 193.

Marusic, I. & Monty, J. P. 2019 Attached eddy model of wall turbulence. *Annu. Rev. Fluid Mech.* **51**, 49–74.

Mizuno, Y. & Jiménez, J. 2013 Wall turbulence without walls. *J. Fluid Mech.* **723**, 429–455.

Park, G. I. & Moin, P. 2014 An improved dynamic non-equilibrium wall-model for large eddy simulation. *Phys. Fluids* **26**, 015108.

Park, G. I. & Moin, P. 2016 Space-time characteristics of wall-pressure and wall shear-stress fluctuations in wall-modeled large eddy simulation. *Phys. Rev. Fluids* **1**, 024404.

Pascarelli, A., Piomelli, U. & Candler, G. V. 2000 Multi-block large-eddy simulations of turbulent boundary layers. *J. Comput. Phys.* **157**, 256–279.

Perry, A. E. & Chong, M. S. 1982 On the mechanism of wall turbulence. *J. Fluid Mech.* **119**, 173–217.

Rozema, W., Bae, H. J., Moin, P. & Verstappen, R. 2015 Minimum-dissipation models for large-eddy simulation. *Phys. Fluids* **27**, 85107.

Sandham, N. D., Johnstone, R. & Jacobs, C. T. 2017 Surface-sampled simulations of turbulent flow at high Reynolds number. *Int. J. Numer. Methods Fluids* **85**, 525–537.

Tennekes, H. & Lumley, J. L. 1972 *A First Course in Turbulence*. MIT Press.

Townsend, A. A. 1976 *The Structure of Turbulent Shear Flow*. Cambridge University Press.

Yang, X. I. A., & Griffin, K. P. 2021 Grid-point and time-step requirements for direct numerical simulation and large-eddy simulation. *Phys. Fluids* **33**, 015108.